Effect of Al2O3, ZnO and TiO2 Atomic Layer Deposition Grown Thin Films on the Electrochemical and Mechanical Properties of Sputtered Al-Zr Coating

Elias Kaady, Roland Habchi, Mikhael Bechelany, Elia Zgheib, Akram Alhussein

▶ **To cite this version:**

Elias Kaady, Roland Habchi, Mikhael Bechelany, Elia Zgheib, Akram Alhussein. Effect of Al2O3, ZnO and TiO2 Atomic Layer Deposition Grown Thin Films on the Electrochemical and Mechanical Properties of Sputtered Al-Zr Coating. Coatings, 2022, 13 (1), pp.65. 10.3390/coatings13010065 . hal-04056013

HAL Id: hal-04056013
https://hal.umontpellier.fr/hal-04056013v1

Submitted on 7 Jun 2023

HAL is a multi-disciplinary open access archive for the deposit and dissemination of scientific research documents, whether they are published or not. The documents may come from teaching and research institutions in France or abroad, or from public or private research centers.

L'archive ouverte pluridisciplinaire **HAL**, est destinée au dépôt et à la diffusion de documents scientifiques de niveau recherche, publiés ou non, émanant des établissements d'enseignement et de recherche français ou étrangers, des laboratoires publics ou privés.

Distributed under a Creative Commons Attribution 4.0 International License

coatings

MDPI

Article

Effect of Al_2O_3, ZnO and TiO_2 Atomic Layer Deposition Grown Thin Films on the Electrochemical and Mechanical Properties of Sputtered Al-Zr Coating

Elias Kaady [1,2,*], Roland Habchi [2], Mikhael Bechelany [3], Elia Zgheib [4] and Akram Alhussein [1,*]

[1] UR LASMIS, Université de Technologie de Troyes, Pôle Technologique Sud Champagne, 52800 Nogent, France
[2] EC2M, Faculty of Sciences, Campus Pierre Gemayel, Lebanese University, Fanar 90656, Lebanon
[3] Institut Européen des Membranes, IEM UMR 5635, Univ Montpellier, CNRS, ENSCM, 34095 Montpellier, France
[4] CIRIMAT, Université de Toulouse, CNRS, INPT, UPS, 4 allée Emile Monso, 31030 Toulouse, France
* Correspondence: elias.kaady@utt.fr (E.K.); akram.alhussein@utt.fr (A.A.)

Abstract: The 316L stainless steels, often used in turbine blades for naval and marine applications, usually suffer from localized pitting corrosion after long exposure to chlorinated environments. The aluminum-zirconium coatings deposited by magnetron sputtering technique can be used to ensure cathodic protection for steels. In this work, we study the influence of atomic layer deposited (ALD) Al_2O_3, ZnO, and TiO_2 thin films on the structural, mechanical, and electrochemical properties of Al-Zr (4 at.% Zr) magnetron sputtered coatings. The morphology, preferred orientation growth, mechanical properties, wettability, and corrosion resistance were investigated. The change in the sputtered Al-Zr morphology is mainly due to the insertion of the ALD layer. The Al-Zr layer deposited on ZnO and TiO_2 layers presented a distinctive morphology. The agglomerate particles of AlZr/Al_2O_3/AlZr, AlZr/ZnO/AlZr and AlZr/TiO_2/AlZr coatings exhibited a cauliflower shape. For ALD/PVD coatings, the insertion of an ALD oxide layer promoted the intensity of the peaks corresponding to the (111) crystallographic orientation. The nanoindentation measurements confirmed the enhancement in the mechanical properties, where the hardness increased by about 75%. The ALD oxide layers promoted the hydrophobicity of the coatings. The electrochemical characterization in a 3.5 wt.% NaCl solution also confirmed the role of the ALD oxides layers in delaying the pitting corrosion of the Al-Zr coating by widening the passive region and enhancing the protective efficiency of the passive film.

Keywords: magnetron sputtering; atomic layer deposition; corrosion; mechanical properties; sacrificial anodes; multilayer coatings

check for updates

Citation: Kaady, E.; Habchi, R.; Bechelany, M.; Zgheib, E.; Alhussein, A. Effect of Al_2O_3, ZnO and TiO_2 Atomic Layer Deposition Grown Thin Films on the Electrochemical and Mechanical Properties of Sputtered Al-Zr Coating. *Coatings* **2023**, *13*, 65. https://doi.org/10.3390/coatings13010065

Academic Editor: Darko Landek

Received: 23 November 2022
Revised: 23 December 2022
Accepted: 27 December 2022
Published: 30 December 2022

Copyright: © 2022 by the authors. Licensee MDPI, Basel, Switzerland. This article is an open access article distributed under the terms and conditions of the Creative Commons Attribution (CC BY) license (https://creativecommons.org/licenses/by/4.0/).

1. Introduction

The austenitic 316L stainless steels are often used in turbine blades for naval and marine applications where a balanced combination of corrosion resistance and mechanical performance is requested [1]. They are also used in a wide range of industrial and domestic applications, such as cutlery, civil structures [1], and biomedical components [2–4]. However, the 316L usually suffers from localized pitting corrosion in chloride ions-rich environments [5,6], and a great number of innovative treatments [1,7,8] are nowadays under intensive study to further improve their corrosion resistance. Sacrificial cathodic protection is an extremely crucial electrochemical method applied across several industries to control the corrosion of steel structures [9,10].

Due to their low cost and high current capacity [10], aluminum (Al) based sacrificial anodes have been employed to protect steels in marine applications. Aluminum coatings deposited by physical vapor deposition (PVD) [11,12] are studied to provide good corrosion resistance properties and to ensure the cathodic protection as long as their open

circuit potential is more negative than that of the steel. However, Al is susceptible to pitting corrosion in chlorinated solutions such as seawater [13]. Chloride ions contribute to the formation of soluble chlorinated aluminum hydroxide, which disrupts the stability of the native Al_2O_3 oxide passivation film on the aluminum surface [13] preventing the thermodynamic stability of Al alloys in a corrosive environment. Alloying other elements with Al anodes was reported [12,14–18] as an adequate method to improve their efficiency. Due to the low solubility of transition metals (TM) in aluminum, the deposition of an extended supersaturated solid solution of TM in aluminum allowed the study of different environmentally friendly aluminum-based alloys' sacrificial anodes. For instance, the effectiveness of alloying aluminum anodes with other TM elements relied on the mechanical reinforcement of the aluminum, the formation of a protective oxide film on the surface and/or the shifting of pitting corrosion potential towards more positive values [17,19]. Among the TM elements, Zirconium (Zr) is a transition metal known as a great grain refiner in traditional aluminum alloys [20–22]. Because of its low electro-negativity and high oxygen affinity compared to Al, Zr considerably improves the corrosion resistance by enriching the protective efficiency of the passive film. When Zr is added, the compactness of alloys increases the Cl^- blocking effect and consequently inhibits the pit propagation. Indeed, zirconium is a passivity promoter that controls the nucleation of pits by delaying the adsorption of chlorides within the aluminum and zirconium oxides passive film [23]. Villardi de Oliveira et al. [20–22] deposited Al–Zr (4 at.% Zr) film by magnetron sputtering to provide sacrificial corrosion resistance of steels. It was a single phased supersaturated solid solution of Zr in Al, presenting the best compromise between the good corrosion behavior and the sacrificial character. Yoshioka et al. [24] investigated the corrosion behavior of sputtered Al-Zr alloys in HCl solution and found that alloying aluminum with zirconium enhanced the pitting corrosion resistance and the passivation ability. Creus et al. [25] classified the Al-based alloys based on their reactivity in saline solution. They reported that increasing the zirconium-alloying element induced the ennoblement of the corrosion potential comparing to pure aluminum. For a 20 wt.% of zirconium content, the Al-Zr coatings ensured the cathodic protection, as their corrosion potentials are more negative than the needed potential threshold. Ma et al. [26] reported the increase of Al coating hardness with zirconium alloying in nanocrystalline film. However, PVD coatings generally exhibit many inherent defects [27] affecting significantly their resistance to corrosion and their toughness. Further investigations are required to enhance the lifetime and the corrosion resistance of the PVD sacrificial anodes. Al-Zr coating is a case study in this work.

Unlike many other vapor-phase deposition techniques, atomic layer deposition (ALD) is not a line-of-sight-dependent process [28]. It allows the deposition of thin films with precise thickness control, excellent uniformity, conformity, and tunable composition [28,29]. Over the last few decades, ALD has emerged as a powerful technique for depositing a variety of thin corrosion-resistant films [1,7,30–32] and for the synthesis of metal oxide composite-based supercapacitor electrodes [33]. Based on a sequential self-limiting surface reactions process, ALD is well known for its ability to deposit highly dense, conformal, and pinhole-free films, which make them attractive candidates for protective barrier applications in aqueous media. Specific oxides thin films are chosen [34] based on their solubility in the working environment, to ensure a considerable corrosion protection. The lower deposition temperature required for most oxidizing reactions promoted the use of ALD oxide ceramic thin films over tougher materials such as nitrides and carbides [35]. For instance, Alumina Al_2O_3 ALD films are the most readily studied ALD thin film for corrosion protection [30–32,34,36]. They present insulating dielectric properties, nucleate well on metals resulting in low porosity and exhibit good diffusion barrier properties. However, in moist environments, Al_2O_3 films eventually fail because they can be slowly converted into aluminum hydroxide, which limits their long-term corrosion protection [36]. Besides, titanium dioxide coating deposited by ALD is also studied as a corrosion protection layer of metals. Titanium dioxide is chemically more stable across a broad pH range and it has been found to decrease the corrosion rate [37–39]. Nevertheless, titanium dioxide

coatings are semiconductors and poor ion barriers, and thus they fail to provide long-term corrosion protection for the underlying metal substrates. Matero et al. [37] studied the corrosion protection of stainless steel by ALD TiO_2 and Al_2O_3 layers and supposed that the conformal ALD coatings could improve the corrosion resistance of different metal alloys. Marin et al. [40] and Shan et al. [38] have studied the corrosion protection of stainless steel using ALD Al_2O_3 and TiO_2 films, where they found that ALD thin films were able to increase the resistance of stainless steel against electrochemical corrosion in NaCl solutions. More recently, ZnO thin films employed as photoelectrodes for solar cells [41], due to their enhanced optical and electrical properties, are now emerging as anticorrosion films. Daubert et al. [34] have investigated the corrosion behavior of ZnO ALD films to protect metals, including copper and stainless steel. Thick ZnO coatings deposited on copper have shown a decreased corrosion current density, which initiated the use of ZnO for anticorrosion applications. However, it was reported that ZnO deposited by ALD suffers from dissolution in purified water.

ALD films can be combined with other anti-corrosion coatings to improve their performance. Several studies were reported on the duplex coatings deposited by PVD and ALD hybrid processes for corrosion protection [8,42–46]. Wan et al. [47] have shown an improvement in corrosion resistance of CrN coatings using ALD Al_2O_3 interlayer. The insertion of the ALD layer is intended to seal the defects of the chemically inert PVD coatings nobler than the substrate and inhibit charge transfer, diffusion of corrosive substances, and dislocation motions. The ALD layers block the trajectory of Cl^- ions towards the substrate, decrease the corrosion current density, and shift the corrosion potential towards more positive values. It shows a new alternative for enhancing the performance and the efficiency of pitting corrosion resistance of the PVD ceramic coatings. In another study, Wan et al. [44] enhanced the corrosion resistance of the CrN coatings by Al_2O_3-TiO_2 nanolaminates sealing layers and found that the improvement in the corrosion resistance revealed in the hybrid PVD+ALD coatings is due to the synergistic effect of Al_2O_3 and TiO_2 acting as excellent passivation barriers to the diffusion of corrosive substances. As it can be seen, the former studies were carried on the hybrid PVD+ALD coatings, where the PVD layer is nobler than substrate. The insertion of the ALD layers aimed to seal PVD layer defects and to act as barriers to the diffusion of corrosive substances. The PVD layer was chemically inert, and once the ALD layer was dissolved, the defects constituted paths towards substrates and the corrosion phenomenon occurred.

In the present work, the concept is different. The PVD layer (Al-Zr) acts as sacrificial anode used for cathodic protection of the steel. Thus, the aluminum coating is gradually consumed over the years according to an electrochemical principle by ensuring the immunity of the steel surface against corrosion. However, the lifetime of this cathodic protection is limited by the consumption time of the coating, and by the current it delivers to the steel. For this, the development of sacrificial anodes having a longer lifetime and a slower consumption rate constitutes the subject and the problem to be treated in this paper. Hence, the present work aims to investigate the influence of the ALD layer on a PVD sacrificial coating less noble than substrate. The effect of Al_2O_3, ZnO and TiO_2 oxide thin films on the structural, mechanical, and electrochemical properties of the Al-Zr (4 at.%) magnetron sputtered coating were studied. Characterization of different hybrid coatings architectures was carried out, in order to determine the possible use of duplex PVD+ALD coatings for the sacrificial protection of stainless steel.

Thus, the combination of the ALD layers with the sputtered Al-Zr coating is in order to:

- Maintain the sacrificial character of the Al-Zr coating and consequently its corrosion potential must always be more electronegative than that of steel. The protection threshold defined by the corrosion potential specific to the steel must not be exceeded.
- Extend the lifetime of the sacrificial coating by widening the passive range and positively shifting the pitting potential with keeping it lower than the corrosion potential of the steel. Thus, localized pitting corrosion of the Al-Zr coating will take place at

higher potentials and the lifetime of the coating will be extended due to the passive film maintaining for a wider potential range, retarding the growth stable pits.
– Improve the mechanical properties of the Al-Zr sacrificial coating that has a weak hardness.

2. Materials and Methods

2.1. Al-Zr Coating Deposition

Al-Zr films were deposited using a DEPHIS4 (Dephis, Etupes, France) magnetron sputtering machine on 316L stainless steel disks (25 mm × 8 mm) and single crystalline Si (100) wafers. The elemental composition of 316L substrates, the procedure of substrate preparation and the sputtering system are well described in our previous study [48]. Prior to the deposition and in order to eliminate surface oxides, the aluminum and zirconium targets (99.99% purity, Φ = 200 mm × 6 mm) were etched with Ar^+ bombardment (0.46 Pa, argon flow rate = 100 sccm) by applying a discharge current of 1 A for 20 min. Al-Zr films were deposited at floating temperature, 0.30 Pa working pressure, and 50 sccm argon flow rate. The discharge voltage and power applied to Al and Zr targets were 273 V-546 W and 174 V-38 W, respectively. The substrate-holder rotation speed was set to 10 rpm. During deposition, neither bias voltage nor substrates heating was performed. The thickness of the Al-Zr layer was controlled by the deposition time as 60, 90, and 150 min for 1, 1.5, and 2.5 µm, respectively.

2.2. Al_2O_3, ZnO, and TiO_2 Atomic Layer Deposition

A custom-made ALD reactor was used to deposit Al_2O_3 and ZnO films using the precursors and the methods adequately described in our previous study [48]. TiO_2 layers were deposited at 150 °C using Titanium (IV) chloride ($TiCl_4$, 99.9% purity, CAS: 7550-45-0, purchased from Sigma-Aldrich, France) and H_2O as precursors. TiO_2 regime consisted of 0.2 s pulse $TiCl_4$, 60 s purge Ar, 2 s pulse H_2O and 60 s purge Ar. The thickness of ALD layers was controlled by the number of ALD cycles. The 50 nm corresponds to 250 cycles of Al_2O_3, 250 cycles for ZnO, and 500 cycles for TiO_2.

2.3. PVD/ALD, ALD/PVD, and PVD/ALD/PVD Architectured Coatings Deposition

Figure 1 represents a schematic illustration that summarizes all the coatings deposited with different architectures named and numbered for simplification. A 50 nm thick layer of Al_2O_3, ZnO, or TiO_2 was deposited on Al-Zr layers for PVD/ALD configuration and as sealing layers for PVD/ALD/PVD configuration. The Al-Zr layers were deposited on these different ALD layers for the ALD/PVD configuration.

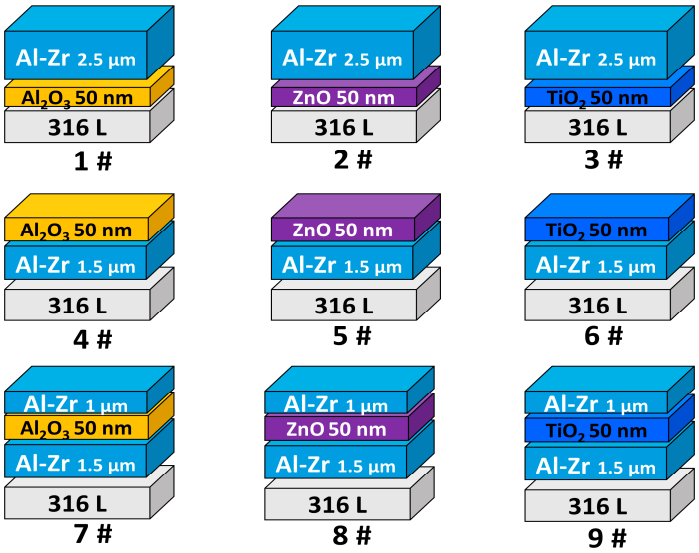

Figure 1. Schematic representation of different coatings architectures.

2.4. Coatings Characterization

The coating morphology and thickness were observed using a FEG Hitachi SU 8030 Scanning Electron Microscope (SEM, Hitachi, Tokyo, Japan). Surface topography was scanned using an atomic force microscopy AFM (Bruker, France) over 2 × 2 μm^2. A Nanoscope Analysis software was used to calculate Rq Roughness from AFM images. Microstructure and crystal phases were identified by an X-ray diffractometer (Bruker D8 advance, Karlsruhe, Germany, XRD) following the procedure described in our previous study [48]. The full width at half maximum (FWHM) as well as the diffraction angle θ were determined after fitting the XRD pattern using a Pseudo-Voigt function. The crystallite size was then determined using Scherrer's formula and the texture coefficients were calculated using TC equation mentioned in our previous study [48].

TriboIndenter TI 980-Hysitron nanoindentation technique (Bruker, MN, USA) equipped with a Berkovich diamond tip (E_{ind} = 1140 GPa, υ_{ind} = 0.07) was used to determine the mechanical properties of the films (Hardness (H) and reduced Young's modulus (E_r)). The maximum penetration depth is limited to 10% of the film thickness in order to avoid the influence of substrate stiffness. Thirty indents were performed for each sample and the average values of H and E_r were calculated. In order to evaluate the hydrophobicity of coatings in humid environments, contact angles were measured using an OCA series machine (Data Physics Model ESr-N, Germany) based on the sessile drop method. Water-droplet profile was acquired using a camera aligned with the samples and a backlighting source. Three measurements were carried out to ensure the reliability of the data.

The electrochemical corrosion properties of samples were evaluated using a potentiostat (Origalys, Rillieux-la-Pape, France) and a flat corrosion cell (BioLogic, Seyssinet-Pariset, France). The corrosion system was well detailed in our previous study [48]. Pitting corrosion tests were performed in a 3.5 wt.% (0.6 M) NaCl solution. In order to ensure system stability, the open circuit potential OCP was measured for 60 min. Corrosion tests were performed in the range of −150 mV/free to 1.3 V/ref. The scan rate was fixed to 0.5 mV/sec.

3. Results

3.1. Coatings Morphology and Surface Topography

SEM images in Figure 2 show the top view morphology of the studied coatings. The observed surface of the as-deposited Al-Zr (4 at.%) coating, presented in Figure 2a, shows the appearance of grains having nodular shapes with eventually visible grain boundaries. This surface topography can predict the presence of porous microstructure. Villardi De Oliveira et al. [20] studied the morphology properties of Al-Zr with different contents of Zr. The coating containing a low amount of Zr presented a columnar growth where the low working pressure of about 0.3 Pa favors the film compactness.

Figure 2b–d presents the top view of the ALD/PVD bilayer with three configurations: Al_2O_3/AlZr, ZnO/AlZr, and TiO_2/AlZr coatings, respectively. The Al-Zr grown on the Al_2O_3 layer presents a similar morphology as the one of Al-Zr grown on steel substrate (Figure 2a) with some triangular prism shape summits noticed between the nodular grains. A change in the microstructure is noticed when the Al-Zr is deposited on ZnO and TiO_2 layers. The observed morphology in Figure 2c indicates that Al-Zr grown on ZnO has a columnar growth with intercolumnar voids, due to the shadowing effect, as reported by Hones' model [49]. This phenomenon indicates that there is still competition between columns, where the highest ones can overgrow the others and create a shadowing effect. On the other side, Figure 2d shows that the Al-Zr grown on TiO_2 presents a distinctive morphology with irregular shapes and dense microstructure. The obtained results confirm that the ALD layer relatively influences the PVD-grown layer. Meanwhile, it has an initial role in the determination of the surface energy, the diffusion mechanism and the mobility control of the nucleated adatoms and islands coalescence during the PVD growth process.

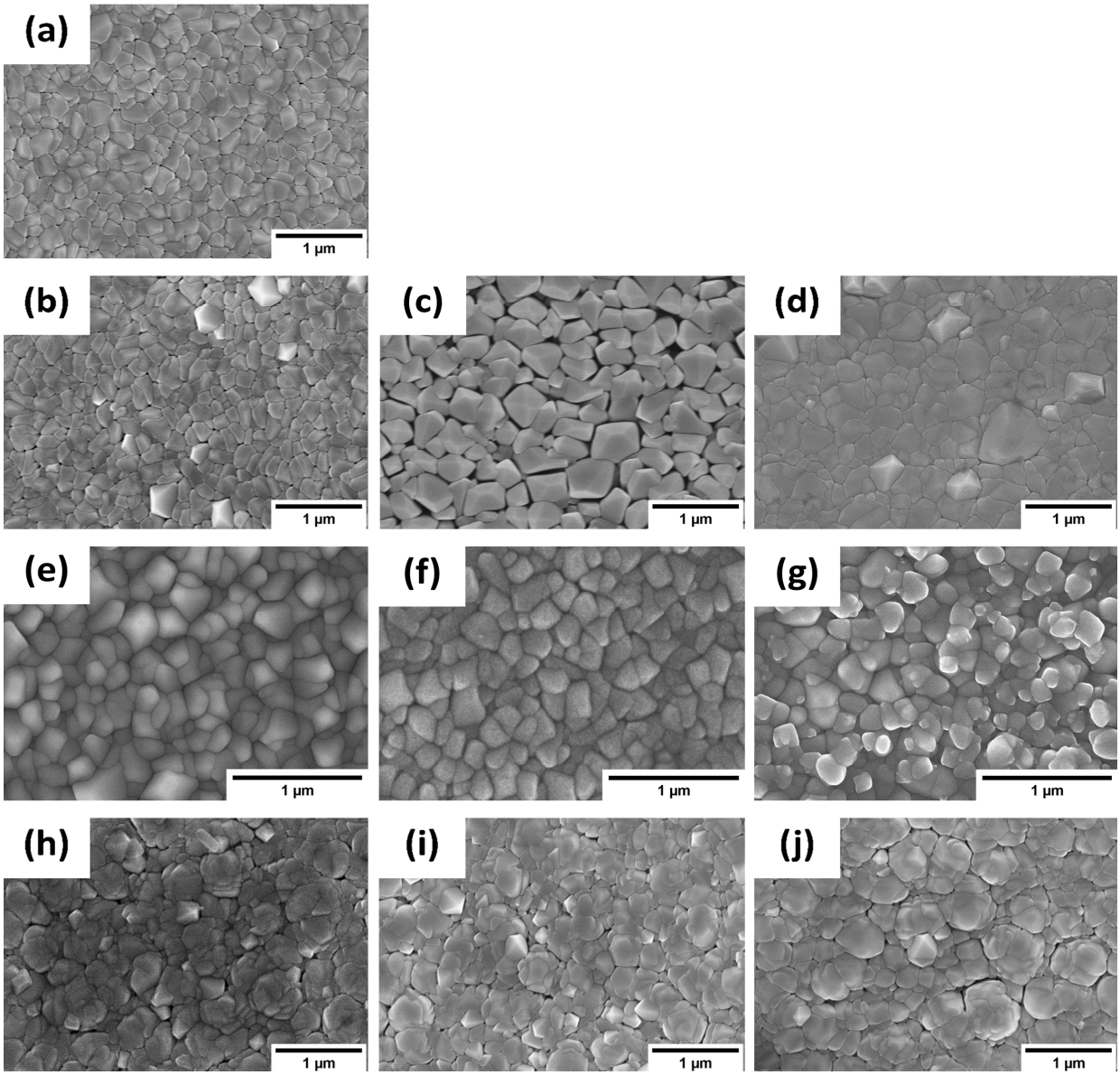

Figure 2. SEM surface images of (**a**) AlZr, (**b**) Al_2O_3/AlZr, (**c**) ZnO/AlZr, (**d**) TiO_2/AlZr, (**e**) AlZr/Al_2O_3, (**f**) AlZr/ZnO, (**g**) AlZr/TiO_2, (**h**) AlZr/Al_2O_3/AlZr, (**i**) AlZr/ZnO/AlZr, and (**j**) AlZr/TiO_2/AlZr.

Figure 2e–g presents the surface morphology of Al_2O_3, ZnO, and TiO_2 ALD thin films deposited on the Al-Zr layer. The ALD layers grew uniformly, conformably, and cover the nodular Al-Zr particles well. Pores or pinholes were no longer observed, which indicates that the ALD layer can seal the defects. The ALD layer smoothed the surface facet and entirely covered the pores and the exposed surface. Voids between columns are filled and the columns are separated by grain boundaries rather than voids.

On the other hand, Figure 2h–j presents the morphology of the top AlZr layer in the PVD/ALD/PVD architectures of AlZr/Al_2O_3/AlZr, AlZr/ZnO/AlZr, and AlZr/TiO_2/AlZr coatings, respectively. The observed morphology is composed of densely distributed agglomerated particles. The nodular shape is still observed but the average size of the nodules is significantly decreased. The shape of agglomerate particles shows a cauliflower appearance. These changes in the coating morphology could be attributed to the ALD interlayer that led to surface modifications with more nucleation sites during the deposition of the Al-Zr layer. Kong et al. [8,50] have previously reported a similar change in the coating

morphology. The insertion of an oxidized ALD interlayer was conducted to the evolution of a pyramid-like morphology to a cauliflower-like surface with a smaller average size of granules.

Figure 3 shows the AFM images of the coatings with the root mean square roughness values (Rq). AFM images confirm the same surface topography observed in the SEM images (Figure 2). Other studies [42,47,48] have reported a decrease in the roughness values after the insertion of an ALD layer in hybrid PVD+ALD coatings that contribute to grain refinement. All of our coatings exhibited an increase in the roughness values, where the morphology of the Al-Zr was changed from a flat surface with nodular particles to the appearance of some triangular prisms on the top of the columns (Figure 3b), a majority of them being of a triangular prismatic shape (Figure 3c) or a cauliflower morphology (Figure 3h–j). The increased difference between the heights of the PVD-grown columns confirms that the ALD layer promotes the shadowing effect and consequently the PVD layer can grow according to Hones' model [49].

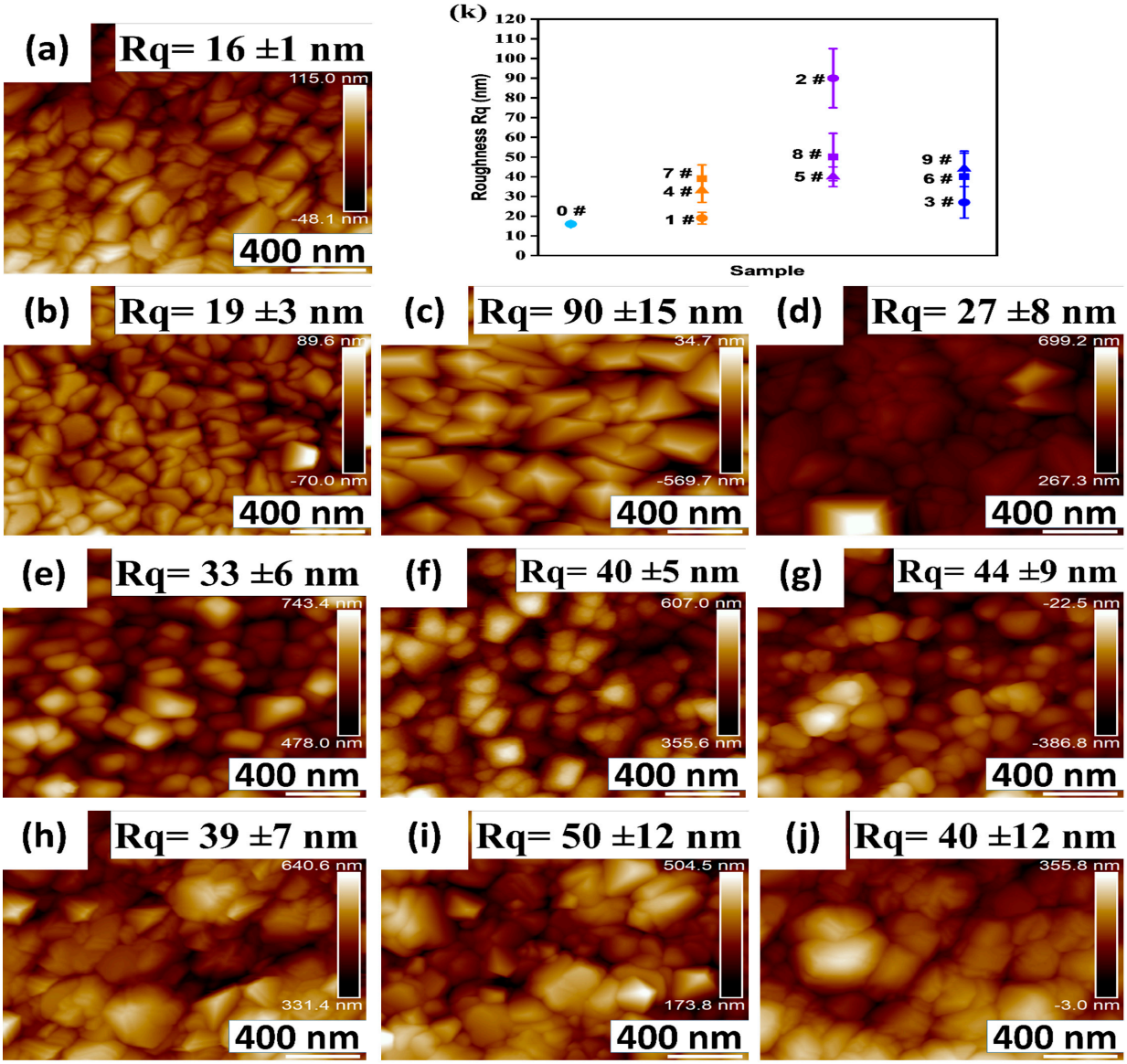

Figure 3. AFM surface images of (**a**) AlZr, (**b**) Al_2O_3/AlZr, (**c**) ZnO/AlZr, (**d**) TiO_2/AlZr, (**e**) AlZr/Al_2O_3, (**f**) AlZr/ZnO, (**g**) AlZr/TiO_2, (**h**) AlZr/Al_2O_3/AlZr, (**i**) AlZr/ZnO/AlZr and (**j**) AlZr/TiO_2/AlZr; (**k**) represents the roughness variation of the different samples. The error bar belongs to the standard deviation of the values.

Figure 4 presents the cross-sectional SEM images of the coatings. All coatings exhibit a columnar growth along their thickness. It can be seen that the width of Al-Zr columns grown on ZnO (Figure 4c) increases compared to that in Figure 4a,b. However, when the Al-Zr coating is deposited on the TiO_2 layer, its morphology becomes relatively compact compared to the other bilayers (Al_2O_3/AlZr and ZnO/AlZr). The 50 nm deposited Al_2O_3, ZnO, and TiO_2 layers can be observed on the top of the Al-Zr films in Figure 4e–g, respectively. The insertion of an ALD sealing layer between two PVD layers (Figure 4h–j) interrupts the continuous film growth and forms a modified surface resulting in the creation of more nucleation sites during the deposition of Al-Zr.

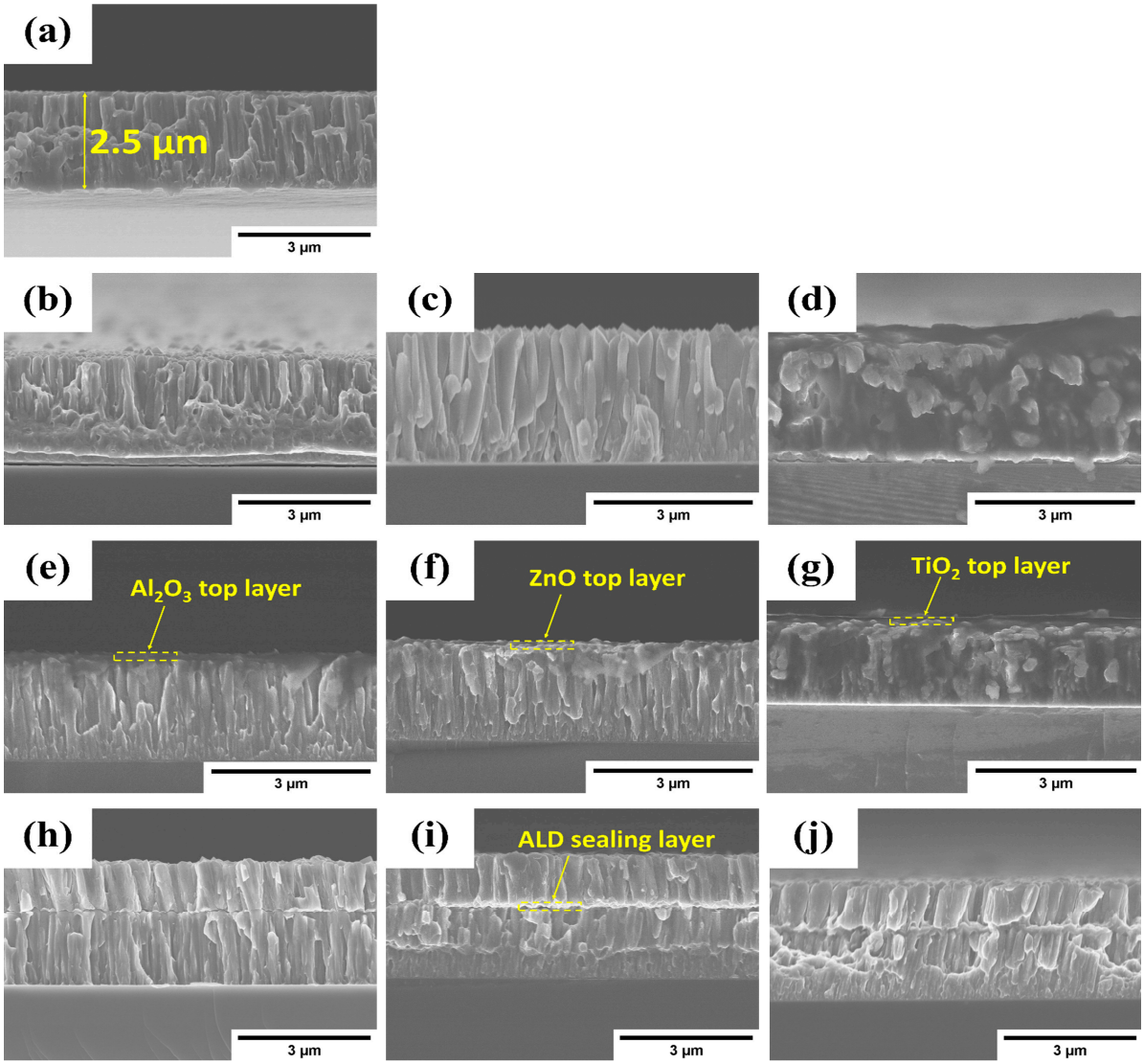

Figure 4. SEM cross-section images of (**a**) AlZr, (**b**) Al_2O_3/AlZr, (**c**) ZnO/AlZr, (**d**) TiO_2/AlZr, (**e**) AlZr/Al_2O_3, (**f**) AlZr/ZnO, (**g**) AlZr/TiO_2, (**h**) AlZr/Al_2O_3/AlZr, (**i**) AlZr/ZnO/AlZr, and (**j**) AlZr/TiO_2/AlZr.

3.2. Structural Analysis

Figure 5a,b presents the XRD patterns of the studied coatings. The Al-Zr (4 at.%) pattern shows the presence of main diffraction peaks at 2θ = 38.34°, 44.5°, 64.8°, and 77.82°, corresponding, respectively, to the (111), (200), (220), and (311) crystallographic planes of the face-centered cubic (fcc) α-Al polycrystalline structure (solid solution supersaturated with Zr). The addition of Zr to the α-Al phase favors the (200) α-Al crystallographic orientation growth. As Zr atomic radius (0.155 nm) is greater than that of Al (0.143 nm),

the lattice parameter increased from 4.059 Å for pure Al (JCPDS File No. 01-089-2837) to 4.066 Å, which is associated with the substitution of aluminum atoms by zirconium ones in the fcc lattice [20]. The XRD patterns of the ALD/PVD, PVD/ALD, and PVD/ALD/PVD coatings are also presented in Figure 5a, respectively. The insertion of an ALD thin film at any position did not provoke any phase transformation in the Al-Zr matrix, as noticed in the XRD patterns.

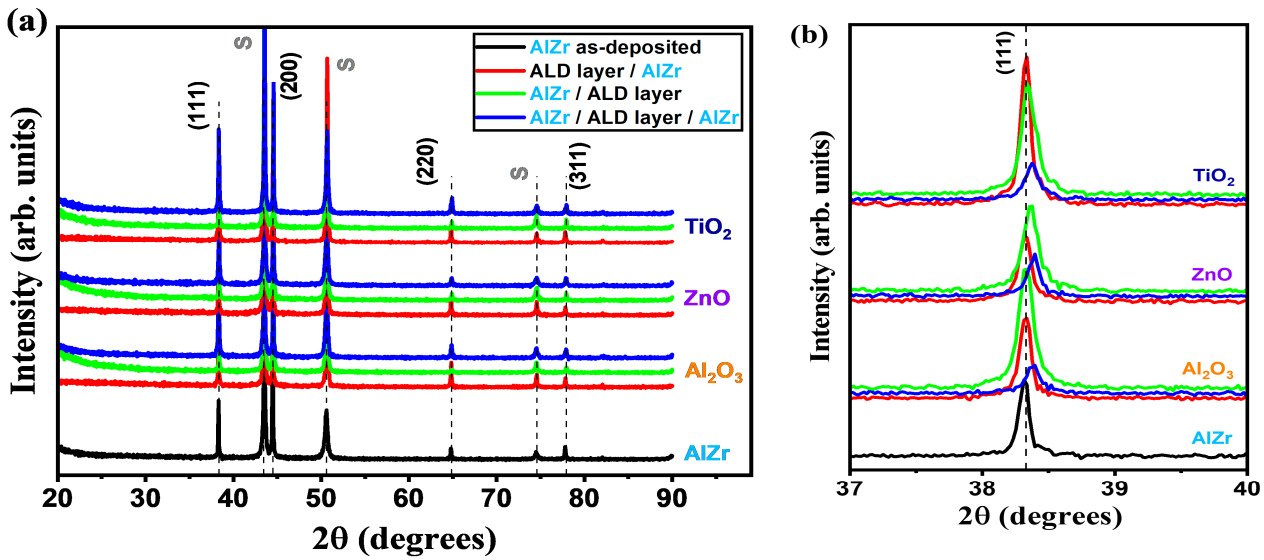

Figure 5. (**a**,**b**) XRD patterns of the coatings.

In order to investigate the texture variation, the texture coefficient (TC) was calculated for the different crystallographic planes as shown in Table 1. Regarding the XRD patterns of ALD/PVD coatings in Figure 5, it can be noticed that the insertion of an ALD oxide layer promotes the intensity of the peaks corresponding to the (111), (220), and (311) orientations, while the intensity of the (200) peak becomes weaker. The Al-Zr grown on TiO_2 presents a higher variation in the texture coefficient where TC of (111) plan increased to 1.18 as shown in Table 1. The variation of TC in PVD/ALD/PVD coatings (Table 1) is less promoted compared to the results observed in the ALD/PVD configurations. Kong et al. [8] have reported the variation of the CrN textured orientation from (111) and (200), to (111) after the insertion of ALD oxide interlayer. This indicates that the ALD layer modified the growth of the Al-Zr layer and induced the growth according to the crystallographic orientation (111) whose texture coefficient remains close to that of the orientation (200). As we had already mentioned, Zr favors the growth of α-Al according to the crystallographic orientation (200). Thus, the decrease in the TC of the (200) orientation when growing on an ALD layer may probably indicate that the effect of Zr in promoting growth according to (200) is reduced. Therefore, the ALD layer could probably create a surface that decreases the mobility and diffusion of Zr atoms in the aluminum lattices during growth. In addition, we notice that the lattice parameter in the hybrid layers decreases slightly to reach a minimum value in the AlZr/ZnO/AlZr coating at 4.061 Å. This can be explained by a decrease in the substitution of Zr in the aluminum lattice due to the reduction in the diffusion of Zr atoms caused by the ALD layer. For all configurations, a decrease in crystallite size is noticed when an ALD layer is present. The size of the crystallites of the 7#, 8# and 9# coatings is of the order of 44 ± 2 nm. Meanwhile, the ALD layer creates more nucleation sites that could suppress the large columnar crystal growth and contribute to crystal refinement [48]. The observed change in texture orientation and crystallite size explain the evolution in coatings morphologies shown in Figures 2 and 4.

Table 1. Lattice parameter, crystallite size, and texture coefficient of samples 0# to 3# and 7# to 9#.

Sample	Lattice Parameter (Å)	Crystallite Size (nm)	Texture Coefficient			
			(111)	(200)	(220)	(311)
0	4.066	58 ± 4	0.37	2.98	0.32	0.33
1	4.065	51 ± 3	0.90	2.12	0.71	0.26
2	4.065	48 ± 3	1.0	2.32	0.42	0.26
3	4.065	49 ± 3	1.18	1.45	0.87	0.50
7	4.064	44 ± 1	0.90	2.15	0.56	0.39
8	4.061	43 ± 2	0.63	2.68	0.35	0.34
9	4.062	44 ± 2	0.70	2.36	0.60	0.34

3.3. Mechanical Properties

Figure 6 presents the mechanical properties of all coatings. Nanohardness (H) and reduced Young's modulus (E_r) were evaluated using the nanoindentation technique. H/E_r and H^3/E_r^2 ratios were then calculated to predict, respectively, the elastic strain and the plastic deformation resistance, which reflect the wear resistance of hard coatings [50]. The larger the H/E_r and H^3/E_r^2 values are, the higher the wear resistance of the coating is [8]. The values of the corresponding data were shown in Table 2.

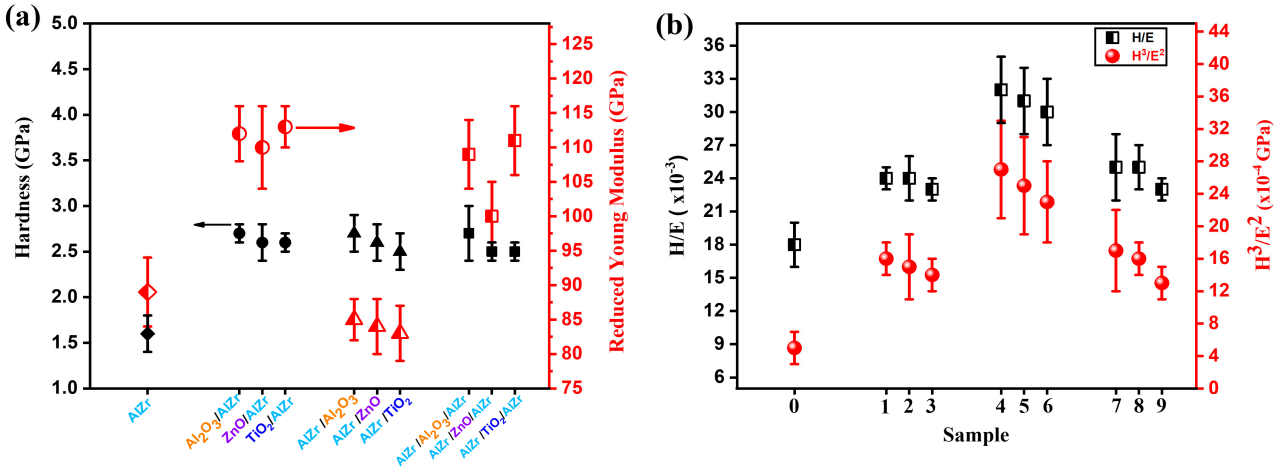

Figure 6. Mechanical properties of coatings. The error bar belongs in (**a**) to the standard deviation and in (**b**) to propagation of errors.

Table 2. H, Er, H/E_r and H^3/E_r^2 values of the coatings.

Sample	0	1	2	3	4	5	6	7	8	9
H (GPa)	1.6 ± 0.2	2.7 ± 0.1	2.6 ± 0.2	2.6 ± 0.1	2.7 ± 0.2	2.6 ± 0.2	2.5 ± 0.2	2.8 ± 0.3	2.5 ± 0.1	2.5 ± 0.1
Er (GPa)	89 ± 5	112 ± 4	110 ± 6	113 ± 3	85 ± 3	84 ± 4	83 ± 4	109 ± 5	100 ± 5	111 ± 5
H/E_r ($\times 10^{-3}$)	18 ± 2	24 ± 1	24 ± 2	23 ± 1	32 ± 3	31 ± 3	30 ± 3	25 ± 3	25 ± 2	23 ± 1
H^3/E_r^2 ($\times 10^{-4}$ GPa)	5 ± 2	16 ± 2	15 ± 4	14 ± 2	27 ± 6	25 ± 6	23 ± 5	17 ± 5	16 ± 2	13 ± 2

The as-deposited Al-Zr coating presented a low hardness H of about 1.6 ± 0.2 GPa, which limits its use and devotes the utility of the combination with ALD oxide layers for improving its mechanical properties. It owns an elastic modulus of 89 ± 5 GPa. The weak mechanical properties of Al-Zr might be attributed to its columnar structure, where the porosity is clearly observed in the SEM images. As shown in Figure 6, all the duplex PVD+ALD coatings exhibit higher hardness. The hardness of the hybrid coatings increases to ~2.7 ± 0.3 GPa (+75%). The Al_2O_3/AlZr, ZnO/AlZr, and TiO_2/AlZr bilayers show an improvement of 69%, 63%, and 63% in hardness values, respectively. The AlZr/Al_2O_3/AlZr, AlZr/ZnO/AlZr, and AlZr/TiO_2/AlZr multilayers also show an improvement in hardness of 75%, 56%, and 56%, respectively. Comparing the different ALD layers, it can be seen that

Al_2O_3 is more effective in the mechanical properties improvement than TiO_2 and ZnO. This confirms the role of the ALD layer insertion in the enhancement of the mechanical properties. The relative enhancement can be attributed to the grain size refinement shown in Table 1, according to the Hall-Petch theory [51]. H/E_r and $H^3/E_r{}^2$ ratios in duplex coatings are higher than those of Al-Zr PVD coatings. Meanwhile, the duplex coatings are stronger and resistant to wear and plastic deformation. The H/E_r and $H^3/E_r{}^2$ ratios increase, respectively, from 0.018 and 5×10^{-4} in AlZr to 0.025 and 17×10^{-4} in the $AlZr/Al_2O_3/AlZr$ configuration. Concurrently, the coating defects can be reduced owing to the good barrier properties of the dense inserted ALD layer. The ALD layers also resist shearing sliding between vertically aligned columnar grains, which enhances the mechanical properties of the Al-Zr coating. Similar improvement in the mechanical properties is observed in other studies [8,46].

3.4. Surface Wettability Behavior

The wettability of a solid surface is related to the surface structure and its chemical state. They play a crucial role in the determination of the interaction between the coating surface and the surrounding environment. In order to understand the coating behavior in a humid environment, the wettability was investigated using contact angle (CA) measurements. Its relationship with the morphology and the corrosion behavior were evaluated. An intrinsic CA below 90° corresponds to a hydrophilic surface, while CA higher than 90° indicates a hydrophobic character. Figure 7 shows the images of contact angles of water droplets dropped on the surfaces of different architectural coatings.

Al-Zr thin film deposited on 316L substrate presents a contact angle CA = 60° ± 2°, which indicates a hydrophilic character. As it can be seen, all the hybrid coatings present a hydrophobic character (CA higher than 90°). The insertion of ALD layers whatever the architecture or the material is, promotes the hydrophobicity of the coating. The change in the wettability behavior is due to the change in the coating morphology, observed in Figure 2.

In our previous study [48], we noticed that the insertion of ALD layer in the (ALD/PVD) hybrid architecture has a low influence on the wettability behavior of the PVD top layer. A slight variation in the CA was observed but the hydrophilicity character of the PVD layer was maintained. This was attributed to the conservation of the PVD layer morphology when grown on ALD layer. In here, the growth of the Al-Zr PVD layer on the ALD layers (Al_2O_3, ZnO and TiO_2) had attributed to a major variation on the Al-Zr PVD grown layer morphology obviously distinguished in Figure 2b–d. The change in the wettability character in these coatings and the transition from the hydrophilicity of Al-Zr (CA = 60° ± 2°) to hydrophobicity (CA = 101° ± 2°, 98° ± 2°, and 95° ± 3° for samples 1#, 2#, and 3#, respectively) is mainly due to the change in the morphology of the PVD top layer.

The hybrid coatings with (PVD/ALD) architecture provided a hydrophobic character with CA = 113° ± 2°, 109° ± 4°, and 104° ± 1° for samples 4#, 5#, and 6#, respectively. The hybrid coatings with (PVD/ALD/PVD) architecture showed the morphologies of densely agglomerated particles with a cauliflower appearance. The water contact angle of samples 7#, 8#, and 9# were 90° ± 4°, 96° ± 6°, and 103° ± 3°, respectively. The ALD layer provoked the change in the morphology of the top PVD layer and thus promoted a PVD structure with hydrophobic character.

All the hybrid coatings with the different architectures presented a change in the wettability character that is mainly due to the morphology evolution. The surface roughness could influence the contact angle, but as it can be seen, its role is secondary as primary one is affected to the morphology parameter. However, no linear relation between roughness and CA variation can be deduced, but it is clear that all the coatings exhibiting higher roughness showed an increase in the water contact angles values.

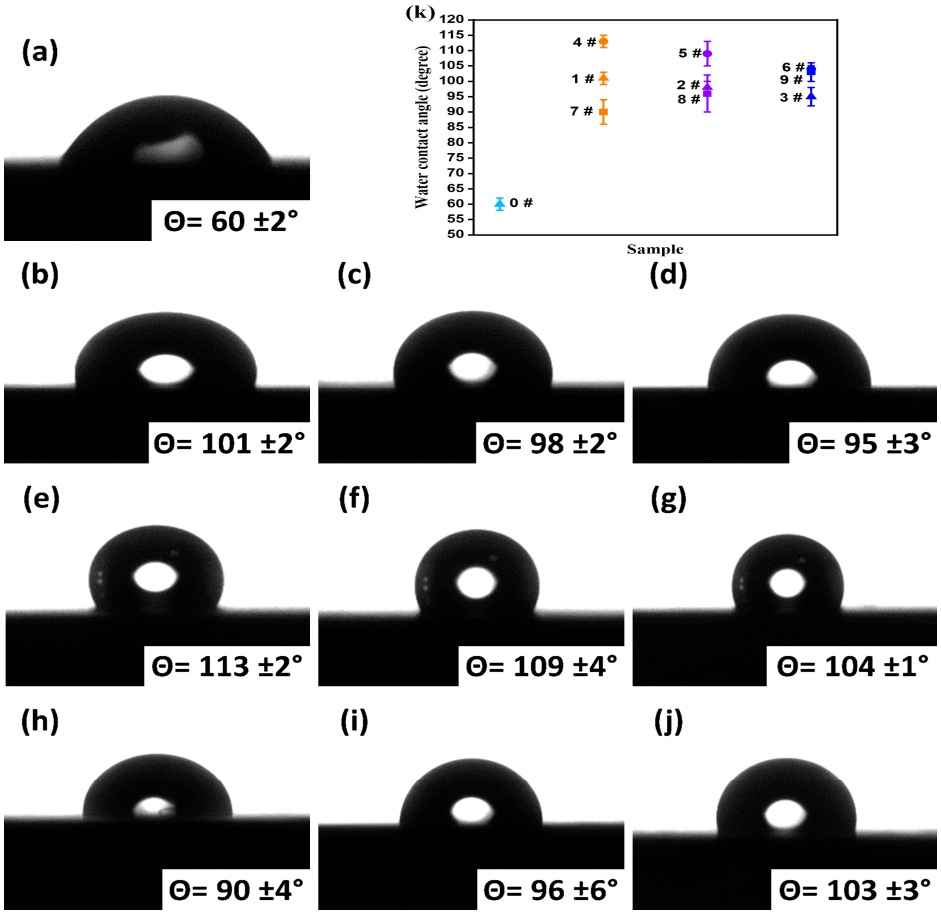

Figure 7. Water contact angle of (**a**) AlZr; (**b**) Al_2O_3/AlZr; (**c**) ZnO/AlZr; (**d**) TiO_2/AlZr; (**e**) AlZr/Al_2O_3; (**f**) AlZr/ZnO; (**g**) AlZr/TiO_2; (**h**) AlZr/Al_2O_3/AlZr; (**i**) AlZr/ZnO/AlZr; and (**j**) AlZr/TiO_2/AlZr. (**k**) The variation of the water contact angles of the coatings. The error bar belongs to standard deviation.

3.5. Corrosion Behavior

The electrochemical behavior of the coatings was investigated in a 3.5 wt.% NaCl solution at room temperature. Figure 8 presents the variation of the open circuit potential (OCP) during 1 h of immersion in the saline solution and the Tafel plots for the different coatings' architectures. The corrosion potential E_{corr} and corrosion current i_{corr} values were determined using the Tafel extrapolation method. E_{pit} represents the potential of pitting corrosion that corresponds to the breakdown of the passive film. Table 3 represents the electrochemical parameters of the different samples.

It can be seen from the polarization curve of 316 L substrate (Figure 8a) that the stainless steel presents a low corrosion density that is due to the formation of Cr_2O_3 passive film. Metastable pits cause current fluctuations between 200 and 400 mV. The passive film is broken down totally at 415 mV and leads to the increase in current density and the growth of stable pits [48].

Al-Zr coating deposited by the PVD technique is less noble than the 316L substrate. Its corrosion potential was found more negative E_{corr} = −670 mV/SCE in comparison with that of 316 L substrate ~162 mV/SCE. The electrochemical curve presents an increase in corrosion current density ~0.6 μA/cm^2 and a narrow passive region. The passive region is followed by an abrupt rise in current at the pitting potential of −485 mV/SCE, which is correlated to the breakdown of the passive film and the beginning of stable pitting corrosion. It has been shown that the Al-Zr coating corrosion was under cathodic control, which reveals sacrificial protection.

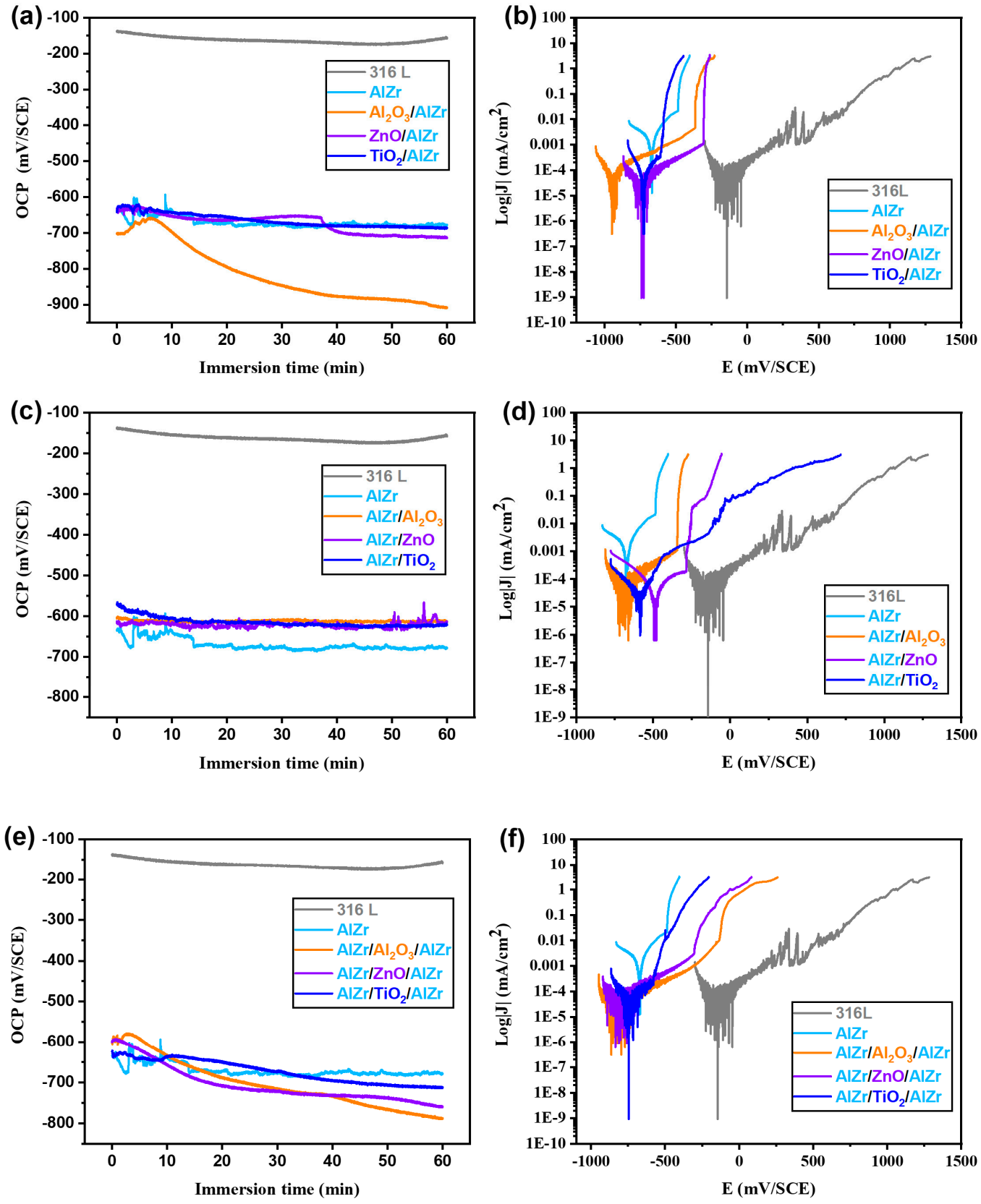

Figure 8. OCP and Tafel plots of the coatings tested in a saline solution (3.5 wt.% NaCl).

Table 3. Corrosion electrochemical parameters of the different samples.

Sample	0	1	2	3	4	5	6	7	8	9
E_{corr} (mV/SCE)	−670	−939	−743	−729	−670	−490	−586	−796	−794	−745
I_{corr} ($\times 10^{-2}$ μA·cm^{-2})	66	5.2	2.8	4.2	1.8	3	2.8	1.4	2.2	2.1
E_{pit} (mV/SCE)	−485	−365	−306	−600	−343	−285	−137	−130	−302	−576
Passivation width (mV/SCE)	115	520	394	90	300	130	290	620	439	134

Figure 8a presents the variation of the OCP potentials of the ALD/PVD bilayers. It is quite clear that the OCP curves of the AlZr and TiO_2/AlZr coatings vary in an almost identical way and have been stabilized around −670 mV/SCE. On the other hand, the ZnO/AlZr coating presents an abrupt decrease in the OCP potential to −700 mV/SCE after 38 min. Al_2O_3/AlZr coating's OCP vary in a different shape of that of the other coatings. It begins at −700 mV/SCE, then shows a slight increase to −670 mV/SCE, and then decreases over time to reach −900 mV/SCE after one hour of immersion. This shape of variation indicates the existence of a protective film dissolving over time. However, the difference between the three behaviors of the ALD layers Al_2O_3, ZnO, and TiO_2 lies in their electrical properties. Indeed, Al_2O_3 is insulator film, while ZnO and TiO_2 are electrical semiconductors. Meanwhile, the Al_2O_3, as an insulator, will block the transfer of charges (electrons) and the electrical contact between the steel and the Al-Zr layer. The galvanic coupling being broken by the Al_2O_3 layer, the following steps take place when the Al_2O_3/AlZr coating is immersed at open circuit for one hour in the saline solution:

- First, the Cl^- ions will adsorb on the passive Zr-enriched film native to the surface of the upper AlZr layer of the Al_2O_3/AlZr coating. The breakdown of this passive film will lead to corrosion of the Al-Zr layer. This is consistent with the increase in the coating OCP from −700 to −670 mV/SCE. At this stage, the steel is susceptible to pitting corrosion, but as the Al_2O_3 layer forms a dense barrier to the way of electrolytes, the steel is protected against corrosion.
- The Al_2O_3 film, being sensitive for dissolution [52] with a dissolution rate which can reach up to 7 ± 1 nm/h in a solution of NaCl [36], dissolves with time. The dissolution of the Al_2O_3 will restore the galvanic coupling between the AlZr and the steel. This may justify the shape of the OCP curve of the Al_2O_3/AlZr coating, which decreases over time and the shift in the corrosion potential towards more negative values than those observed with the ZnO/AlZr and TiO_2/AlZr coatings.
- Following the dissolution of the Al_2O_3 layer, the AlZr layer corrodes for the sacrifice of the steel and the transfer of charges (electrons) to the steel will be restored.

However, the process established with the ZnO and TiO_2 layers is different from that carried out by Al_2O_3 because they are electrical semiconductors. Consequently, the galvanic coupling is ensured before the dissolution of these layers or their rupture. Nevertheless, the charge transfer between steel and Al-Zr is more difficult. For this reason, we can see that the variations in their corresponding OCP curves are almost similar to that of the AlZr coating.

Figure 8b presents the electrochemical behaviors of the ALD/PVD bilayers deposited on the 316L substrate. The insertion of the ALD oxide layer between the substrate and the PVD Al-Zr layer shifts the corrosion potential towards a more negative value than whatever the ALD layer material is (Al_2O_3, ZnO or TiO_2). Due to the galvanic coupling between the steel and the Al-Zr layer, the substrate-coating interface, in the presence of electrolytes, constitutes the zone where the corrosion phenomenon will take place. Inserting an interfacial ALD oxide layer at the substrate-coating interface will seal most of the substrate surface and impede oxygen access to this area. The cathodic shift (towards more negative values) observed in the corrosion potential could be attributed to the phenomenon of blocking up the oxygen diffusion to the substrate-coating interface. As the oxygen is the promoter of the water reduction reaction, inhibiting its diffusion will limit this reduction. As it was proposed by Mirhashemihaghighi et al. [32], the higher density of ALD coating

combined with its higher thickness (50 nm) may hinder the access of water (and oxygen) to the coating/substrate interface. Diffusion of oxygen remains more difficult at the interface, thanks to the thicker and denser ALD coating, which leads to a decrease in the corrosion potential and thus shifts E_{corr} towards values that are more negative. In addition, another reason for this E_{corr} cathodic shift could be attributed to the pH effect. The increase in the concentration of hydroxide ions OH^-, products of the water reduction reaction, at the substrate-coating interface leads to an increase in the pH at this zone and consequently to the destabilization of the ALD oxide film [32]. The dissolution of this film causes the increase of the anodic corrosion current and thus the corrosion potentially shifts towards more negative values.

The three ALD/PVD coatings show a decrease in the corrosion current density. Active-passive transition is not observed, which indicates that the passive film formation takes place during the cathodic polarization. The Al_2O_3 and ZnO insertion enlarged the width of the passive domain to 520 and 394 mV/SCE, respectively. The passive current density decreases compared to that of the AlZr coating, which indicates an improvement in the effectiveness of the protective film and, therefore, a more stable resistance to pitting corrosion. The inserted TiO_2 layer did not cause a similar widening in the width of the passive region. This could be attributed to the specific microstructure of the Al-Zr deposited on TiO_2, which may be more sensitive to nucleation and pit growth due to the heterogeneous distribution of particles differing in size and shape (Figure 2d).

Figure 8c shows the PVD/ALD coatings' OCP variation. It is obvious that all the three coatings exhibit the stabilization of the free potential at higher potentials than that of the AlZr coating. The Tafel plots of PVD/ALD coatings are shown in Figure 8d. The electrochemical curve of the AlZr/Al_2O_3 coating shows a very low corrosion current density ~18 nA·cm^{-2} in the same corrosion potential range of the AlZr coating. The deposition of the upper Al_2O_3 ALD layer led to the decrease of the corrosion current density and the broadening of the passivity region, thereby shifting the pitting corrosion potential to higher value E_{pit} ~ −343 mV/SCE. The tafel plots of the AlZr/ZnO and AlZr/TiO_2 coatings show positive shifts in the corrosion potentials. The fact that the dense ALD layer constitutes a chemical barrier reducing the number of sites available for the attack of the Al-Zr layer by the Cl^- ions, and thus shifting the corrosion potential towards more positive values. A decrease in the corrosion current density is observed. This can be explained by the direct contact of the ALD layer with its corrosive environment. The ALD oxide layer hinders the adsorption effect of Cl^- ions. It is well known [19] that the pitting mechanism is directly related to the adsorption of chloride anions on the surface of the passive film, and the stable growth of pits occurs with the increase of chloride ions concentration. The high protective and barrier performance of the ALD layer blocks the adsorption of Cl^- ions on the surface and decreases the dissolution of the Al-Zr layer by shifting the corrosion potential to a more positive value and thus delaying the onset of stable pits growth. The passive domain of the AlZr/Al_2O_3 coating is wider (~300 mV/SCE) than those of AlZr/ZnO and AlZr/TiO_2. Meanwhile, Al_2O_3 is more effective in promoting more stable passive layer (passivation domain).

The OCP and Tafel curves of the PVD/ALD/PVD coatings are shown in Figure 8e,f. It is noticed that the OCP curves of the three hybrid coatings in Figure 8e take a decreasing trend indicating a dissolution of the protective film. The OCP potential of the three hybrid coatings was initially higher than that of the Al-Zr coating then decreases over time to remain more negative. At the beginning of the immersion in the NaCl solution, the OCP potential of the PVD/ALD/PVD hybrid coatings was higher than that of the Al-Zr coating and quite similar to the results of PVD/ALD coatings' OCP results. Thus, it can be seen that the first mechanism, which contributed to that shift towards more positive values, is the decrease in the available sites for the Cl^- ions adsorption. The ALD layer acted as a barrier to Cl^- ions diffusion. With the ALD layer dissolution over time, the dominant phenomenon changed from that of the adsorption of Cl^- ions to the blocking of the oxygen diffusion. Thus, the water reduction is limited, which causes a shift in the OCP potential towards

more negative values than that of the Al-Zr coating. A similar behavior to the results obtained with the ALD/PVD coatings (Figure 8a). According to the Tafel plots, Figure 8f, all the ALD coatings led to the shift of the corrosion potential towards more negative values and to a decrease in the corrosion current density. The AlZr/Al_2O_3/AlZr coating has the lowest corrosion density among all other coatings (14 nA·cm^{-2}). Likewise, it has the widest passive range ~620 mV/SCE among the others. The insertion of the ZnO layer by ALD also enlarged the passive domain to 439 mV/SCE while TiO_2 represents the weakest enlargement 134 mV/SCE close to that of the as-deposited AlZr coating (115 mV/SCE).

Mohamed et al. [53] reported that super hydrophobic coatings prevent metal substrates from corroding due to air retained on these surfaces. The retained air can prevent corrosive substances, for example chloride ions from seawater, from attacking the surface of the substrate, providing an effective new anti-corrosion mechanism. A large amount of air retained between the valleys of the rough structure prevents the infiltration of corrosive ions such as Cl^- and thus slows down the breakdown of the oxide layer of the passive film. Additionally, the retained air prevents the metal surface from corroding and attributes to the excellent anti-corrosion properties of the film. Thus, relating the coatings wettability character to their electrochemical behaviors, it is noticed that the hydrophobicity caused the decrease of the corrosion current density and the passive current density of all the hybrid coatings, which may indicate a decrease in the corrosion rate and a slowing down of the passive layers breakdown. Therefore, the character hydrophobic generated by the insertion of the ALD layer with the PVD layer has contributed to the improvement of the anti-corrosion properties of the films.

Regarding the corrosion potential of the various PVD+ALD hybrid coatings, it can be seen that the combination of the ALD layer with PVD never led to an increase in E_{corr} greater than that of the 316L substrate. The E_{corr} shifted towards more negative (ALD/PVD and PVD/ALD/PVD architectures) or positive (PVD/ALD architecture) values compared to the E_{corr} of the AlZr PVD coating. All PVD+ALD hybrid coatings exhibited lower corrosion densities than the AlZr coating, indicating a slowing down of the corrosion rate due to the addition of an ALD layer. The ALD layer material and the position in which it is disposed in the hybrid architecture, are initial parameters that determine the mechanism by which the ALD layer will influence the passive domain and the pitting potential of the coating. Therefore, the hybrid coatings exhibited different passive region width and pitting corrosion potentials.

For the TiO_2/AlZr coating, it is noticed that, despite the advantage of shifting the corrosion potential towards lower value, the reduction in the passive domain width and the lower pitting potential (−600 mV/SCE) than that of the AlZr coating (−485 mV/SCE) limited its improvement of the AlZr efficiency. The similar limitation was observed with the insertion of the TiO_2 layer in the PVD/ALD/PVD architecture where the pitting potential is −576 mV/SCE. On the other hand, the AlZr/TiO_2 coating presented the disadvantage of delaying the pitting corrosion potential (−137 mV/SCE) near to E_{corr} of 316L substrate (−162 mV/SCE), which may possibly cause a loss of the sacrificial character of the coating. Thus, the TiO_2 deposited by ALD only presented the advantage of decreasing the corrosion density.

For the ZnO, it is noticed that the insertion of this ALD layer widened the passive domain whatever its position. The AlZr/ZnO/AlZr coating exhibits passive domain broader than those observed in the ZnO/AlZr and AlZr/ZnO coatings. The pitting potentials of these three coatings are in the same potential range ~ −300 ± 20 mV/SCE, lower than the E_{corr} of the substrate indicating the conservation of the sacrificial character of the coatings. The PVD/ALD/PVD architecture is more recommended than the others, thanks to the advantage of the wider passive domain.

For Al_2O_3, the AlZr/Al_2O_3/AlZr coating widened the passive domain and extended the pitting potential to −130 mV/SCE close to E_{corr} of the substrate, which can probably lead to the loss of the sacrificial character of this coating. On the other hand, the Al_2O_3/AlZr coating presents a significant broadening of the passive domain with a pitting potential at

−365 mV/SCE with retaining its sacrificial character. The passive region is four times larger than that of the as deposited AlZr coating, indicating the effectiveness of the hybrid PVD and ALD combination in slowing down the consumption of the sacrificial coating and extending its lifetime. The ALD/PVD and PVD/ALD/PVD architectures were more efficient than the PVD/ALD architecture. Comparing the ALD/PVD and PVD/ALD/PVD architectures, it seems difficult to recommend one over the other, since the hybrid combination always depends on the ALD material type with respecting the conservation of the sacrificial character. However, it is possible to recommend Al_2O_3/AlZr and AlZr/ZnO/AlZr coatings without denying the effectiveness of other coatings that have maintained their sacrificial characteristics with lower corrosion density.

4. Conclusions

In this work, we have investigated the mechanical and electrochemical performance of Al-Zr coating deposited by magnetron sputtering and altered with three oxide thin films: Al_2O_3, ZnO, and TiO_2, deposited by ALD technique. Three main configurations were studied in this paper: PVD/ALD, ALD/PVD, and PVD/ALD/PVD. The morphology of the Al-Zr grown on an ALD oxide layer was well influenced by the ALD film material and position. The Al-Zr layer deposited on ZnO and TiO_2 layers presents a distinctive morphology. The agglomerate particles of AlZr/Al_2O_3/AlZr, AlZr/ZnO/AlZr, and AlZr/TiO_2/AlZr coatings present a cauliflower shape. All coatings exhibit an increase in the roughness values.

Microstructure evolution was also observed. For ALD/PVD coatings, the insertion of an ALD oxide layer promotes the intensity of the peaks corresponding to the (111) crystallographic orientation. All the duplex PVD+ALD coatings exhibit higher hardness than the as-deposited AlZr PVD coating. The hardness in the hybrid coating increases to 2.7 GPa (75%). Comparing the different ALD layers, Al_2O_3 was more effective in the mechanical properties improvement than TiO_2 and ZnO. The insertion of an ALD oxide layer whatever the architecture or the material is, promotes the hydrophobicity of coating.

Inserting an ALD oxide layer between the 316L substrate and the Al-Zr PVD layer led to shift the corrosion potential to a lower negative value. Al_2O_3 (ALD) layer insertion was more effective than ZnO and TiO_2 in improving the sacrificial character of Al-Zr for steel protection. In the PVD/ALD/PVD architecture, all the ALD layers led to shift the corrosion potentials towards higher positive values, a further decrease in the passive current density and a widening of the passive potential range. Al_2O_3/AlZr and AlZr/ZnO/AlZr coatings are recommended as excellent candidates representing good sacrificial character to slow down the consumption rate of AlZr and extend its service life for the protection of 316L steel. However, this does not deny the effectiveness of other sacrificial coatings with lower corrosion density than the AlZr coating. In this work, the combination of both PVD and ALD deposition processes showed a great industrial potential for future advanced coatings. The number of coating layers and materials present the following step of this study to enhance the performance of a hybrid multi layered coating.

Author Contributions: Conceptualization, A.A. and R.H.; methodology, E.K., A.A. and R.H.; software, E.K. and E.Z.; formal analysis, E.K.; investigation, E.K., E.Z. and M.B.; Resources, A.A. and M.B.; data curation, E.K. and A.A.; writing—original draft preparation, E.K.; writing—review and editing, R.H., M.B., E.Z. and A.A.; supervision, A.A. and R.H.; Validation, A.A., R.H. and M.B.; Project administration, A.A. All authors have read and agreed to the published version of the manuscript.

Funding: This research was funded, within DRAPED project, by FEDER and UT/INSA-UL Network.

Institutional Review Board Statement: Not applicable.

Informed Consent Statement: Not applicable.

Data Availability Statement: Data is contained within the article.

Acknowledgments: The authors would like to thank Cassandre Lamboux and Syreina Sayegh for their help in ALD technical support. The authors would also like to thank the European Union (Fond Européen de Développement Régional) and the Doctoral School in Sciences and Technology at the Lebanese University (Réseau UT/INSA-UL) for their financial support. This work was performed within DRAPED project.

Conflicts of Interest: The authors declare no conflict of interest.

References

1. Marin, E.; Lanzutti, A.; Paussa, L.; Guzman, L.; Fedrizzi, L. Long term performance of atomic layer deposition coatings for corrosion protection of stainless steel. *Mater. Corros.* **2015**, *66*, 907–914. [CrossRef]
2. Bordji, K.; Jouzeau, J.-Y.; Mainard, D.; Payan, E.; Delagoutte, J.-P.; Netter, P. Evaluation of the effect of three surface treatments on the biocompatibility of 316L stainless steel using human differentiated cells. *Biomaterials* **1996**, *17*, 491–500. [CrossRef]
3. Mojarad Shafiee, B.; Torkaman, R.; Mahmoudi, M.; Emadi, R.; Derakhshan, M.; Karamian, E.; Tavangarian, F. Surface modification of 316L SS implants by applying bioglass/gelatin/polycaprolactone composite coatings for biomedical applications. *Coatings* **2020**, *10*, 1220. [CrossRef]
4. Staszuk, M.; Pakuła, D.; Reimann, Ł.; Kloc-Ptaszna, A.; Pawlyta, M.; Kříž, A. Structure and properties of TiO_2/NanoTiO_2 bimodal coatings obtained by a hybrid PVD/ALD method on 316L steel substrate. *Materials* **2021**, *14*, 4369. [CrossRef] [PubMed]
5. Nie, J.; Wei, L.; Jiang, Y.; Li, Q.; Luo, H. Corrosion mechanism of additively manufactured 316 L stainless steel in 3.5 Wt.% NaCl solution. *Mater. Today Commun.* **2021**, *26*, 101648. [CrossRef]
6. Sander, G.; Cruz, V.; Bhat, N.; Birbilis, N. On the in-situ characterisation of metastable pitting using 316L stainless steel as a case study. *Corros. Sci.* **2020**, *177*, 109004. [CrossRef]
7. Marin, E.; Lanzutti, A.; Lekka, M.; Guzman, L.; Ensinger, W.; Fedrizzi, L. Chemical and mechanical characterization of TiO_2/Al_2O_3 atomic layer depositions on AISI 316 L stainless steel. *Surf. Coat. Technol.* **2012**, *211*, 84–88. [CrossRef]
8. Kong, J.; Li, C.; Sun, X.; Xuan, Y.; Zhai, H.; Li, A.; Wang, Q.; Zhou, F. Improved tribological properties and corrosion protection of CrN coating by ultrathin composite oxide interlayer. *Appl. Surf. Sci.* **2021**, *541*, 148606. [CrossRef]
9. Pedeferri, P. Cathodic and anodic protection. In *Corrosion Science and Engineering*; Springer: Berlin/Heidelberg, Germany, 2018; pp. 383–422. [CrossRef]
10. Xi, Y.; Jia, M.; Zhang, J.; Zhang, W.; Yang, D.; Sun, L. Evaluating the performance of aluminum sacrificial anodes with different concentration of gallium in artificial sea water. *Coatings* **2022**, *12*, 53. [CrossRef]
11. Navinšek, B.; Panjan, P.; Milošev, I. PVD Coatings as an environmentally clean alternative to electroplating and electroless processes. *Surf. Coat. Technol.* **1999**, *119*, 476–487. [CrossRef]
12. Perez, A.; Billard, A.; Rébéré, C.; Berziou, C.; Touzain, S.; Creus, J. Influence of metallurgical states on the corrosion behaviour of Al–Zn PVD coatings in saline solution. *Corros. Sci.* **2013**, *74*, 240–249. [CrossRef]
13. Sukiman, N.L.; Zhou, X.; Birbilis, N.; Hughes, A.E.; Mol, J.M.C.; Garcia, S.J.; Thompson, G.E. Durability and corrosion of aluminium and its alloys: Overview, property space, techniques and developments. In *Aluminium Alloys—New Trends in Fabrication and Applications*; IntechOpen: London, UK, 2013; ISBN 978-953-51-0861-0.
14. Sanchette, F.; Czerwiec, T.; Billard, A.; Frantz, C. Sputtering of Al-Cr and Al-Ti composite targets in pure Ar and in reactive Ar-N_2 plasmas. *Surf. Coat. Technol.* **1997**, *96*, 184–190. [CrossRef]
15. Sanchette, F.; Billard, A.; Frantz, C. Mechanically reinforced and corrosion-resistant sputtered amorphous aluminium alloy coatings. *Surf. Coat. Technol.* **1998**, *98*, 1162–1168. [CrossRef]
16. Sanchette, F.; Billard, A. Main features of magnetron sputtered aluminium–transition metal alloy coatings. *Surf. Coat. Technol.* **2001**, *142–144*, 218–224. [CrossRef]
17. Creus, J.; Billard, A.; Sanchette, F. Corrosion behaviour of amorphous Al–Cr and Al–Cr–(N) coatings deposited by Dc magnetron sputtering on mild steel substrate. *Thin Solid Films* **2004**, *466*, 1–9. [CrossRef]
18. Perez, A.; Sanchette, F.; Billard, A.; Rébéré, C.; Berziou, C.; Touzain, S.; Creus, J. Comparison of the intrinsic properties of EBPVD Al–Ti and Al–Mg coatings. *Mater. Chem. Phys.* **2012**, *132*, 154–161. [CrossRef]
19. Reffass, M.; Berziou, C.; Rébéré, C.; Billard, A.; Creus, J. Corrosion behaviour of magnetron-sputtered Al_{1-x}–Mn_x coatings in neutral saline solution. *Corros. Sci.* **2010**, *52*, 3615–3623. [CrossRef]
20. Villardi de Oliveira, C. Development of Multifunctional Coatings Combining Anticorrosion and Antibiofouling Properties. Ph.D. Thesis, Université de Technologie de Troyes, Troyes, France, 2019. NNT: 2019TROY0034. Available online: https://theses.hal.science/tel-03624526 (accessed on 10 October 2022).
21. Villardi de Oliveira, C.; Migot, S.; Alhussein, A.; Jiménez, C.; Schuster, F.; Ghanbaja, J.; Sanchette, F. Structural and microstructural analysis of bifunctional TiO_2/Al-Zr thin film deposited by hybrid process. *Thin Solid Films* **2020**, *709*, 138255. [CrossRef]
22. Villardi de Oliveira, C.; Alhussein, A.; Creus, J.; Schuster, F.; Schlegel, M.L.; Dong, Z.; Jiménez, C.; Sanchette, F. Bifunctional TiO_2/AlZr thin films on steel substrate combining corrosion resistance and photocatalytic properties. *Coatings* **2019**, *9*, 564. [CrossRef]

23. Perez, A. Influence de La Nanostructuration Sur Le Comportement à La Corrosion de Revêtements Multicouches Élaborés Par PVD. Ph.D. Thesis, Université de La Rochelle, La Rochelle, France, 2011. NNT: 2011LAROS334. Available online: https://theses.hal.science/tel-00697016 (accessed on 10 October 2022).
24. Yoshioka, H.; Habazaki, H.; Kawashima, A.; Asami, K.; Hashimoto, K. The corrosion behavior of sputter-deposited Al-Zr alloys in 1 M HCl solution. *Corros. Sci.* **1992**, *33*, 425–436. [CrossRef]
25. Creus, J.; Berziou, C.; Cohendoz, S.; Perez, A.; Rébéré, C.; Reffass, M.; Touzain, S.; Allely, C.; Gachon, Y.; Héau, C.; et al. Reactivity classification in saline solution of magnetron sputtered or EBPVD pure metallic, nitride and Al-based alloy coatings. *Corros. Sci.* **2012**, *57*, 162–173. [CrossRef]
26. Ma, B.; Qi, X.; Li, R.; Zhang, R.; Shang, H. The Zr alloying effect on microstructure evolution and mechanical properties of nanostructured Al-Zr alloyed films. *J. Alloys Compd.* **2021**, *858*, 157707. [CrossRef]
27. Panjan, P.; Drnovšek, A.; Gselman, P.; Čekada, M.; Panjan, M. Review of growth defects in thin films prepared by PVD techniques. *Coatings* **2020**, *10*, 447. [CrossRef]
28. Cremers, V.; Puurunen, R.L.; Dendooven, J. Conformality in atomic layer deposition: Current status overview of analysis and modelling. *Appl. Phys. Rev.* **2019**, *6*, 021302. [CrossRef]
29. George, S.M. Atomic layer deposition: An overview. *Chem. Rev.* **2010**, *110*, 111–131. [CrossRef]
30. Potts, S.E.; Schmalz, L.; Fenker, M.; Díaz, B.; Światowska, J.; Maurice, V.; Seyeux, A.; Marcus, P.; Radnóczi, G.; Tóth, L.; et al. Ultra-thin aluminium oxide films deposited by plasma-enhanced atomic layer deposition for corrosion protection. *J. Electrochem. Soc.* **2011**, *158*, 132–138. [CrossRef]
31. Díaz, B.; Härkönen, E.; Światowska, J.; Seyeux, A.; Maurice, V.; Ritala, M.; Marcus, P. Corrosion properties of steel protected by nanometre-thick oxide coatings. *Corros. Sci.* **2014**, *82*, 208–217. [CrossRef]
32. Mirhashemihaghighi, S.; Światowska, J.; Maurice, V.; Seyeux, A.; Zanna, S.; Salmi, E.; Ritala, M.; Marcus, P. Corrosion protection of aluminium by ultra-thin atomic layer deposited alumina coatings. *Corros. Sci.* **2016**, *106*, 16–24. [CrossRef]
33. Ansari, M.Z.; Seo, K.-M.; Kim, S.-H.; Ansari, S.A. Critical aspects of various techniques for synthesizing metal oxides and fabricating their composite-based supercapacitor electrodes: A review. *Nanomaterials* **2022**, *12*, 1873. [CrossRef]
34. Daubert, J.S.; Hill, G.T.; Gotsch, H.N.; Gremaud, A.P.; Ovental, J.S.; Williams, P.S.; Oldham, C.J.; Parsons, G.N. Corrosion protection of copper using Al_2O_3, TiO_2, ZnO, HfO_2, and ZrO_2 atomic layer deposition. *ACS Appl. Mater. Interfaces* **2017**, *9*, 4192–4201. [CrossRef]
35. Marin, E.; Fedrizzi, L. Atomic layer deposition an innovative technology to improve corrosion and surface functionalities of alloys. In *Encyclopedia of Interfacial Chemistry*; Elsevier: Amsterdam, The Netherlands, 2018; pp. 79–89, ISBN 9780124095472.
36. Díaz, B.; Härkönen, E.; Maurice, V.; Światowska, J.; Seyeux, A.; Ritala, M.; Marcus, P. Failure mechanism of thin Al_2O_3 coatings grown by atomic layer deposition for corrosion protection of carbon steel. *Electrochim. Acta* **2011**, *56*, 9609–9618. [CrossRef]
37. Matero, R.; Ritala, M.; Leskelä, M.; Salo, T.; Aromaa, J.; Forsén, O. Atomic layer deposited thin films for corrosion protection. *Le J. Phys. IV* **1999**, *09*, 493–499. [CrossRef]
38. Shan, C.X.; Hou, X.; Choy, K.-L. Corrosion resistance of TiO_2 films grown on stainless steel by atomic layer deposition. *Surf. Coat. Technol.* **2008**, *202*, 2399–2402. [CrossRef]
39. Merisalu, M.; Aarik, L.; Kozlova, J.; Mändar, H.; Tarre, A.; Sammelselg, V. Effective corrosion protection of aluminum alloy AA2024-T3 with novel thin nanostructured oxide coating. *Surf. Coat. Technol.* **2021**, *411*, 126993. [CrossRef]
40. Marin, E.; Lanzutti, A.; Guzman, L.; Fedrizzi, L. Corrosion protection of AISI 316 stainless steel by ALD alumina/titania nanometric coatings. *J. Coat. Technol. Res.* **2011**, *8*, 655–659. [CrossRef]
41. Alam, M.W.; Ansari, M.Z.; Aamir, M.; Waheed-Ur-Rehman, M.; Parveen, N.; Ansari, S.A. Preparation and characterization of Cu and Al doped ZnO thin films for solar cell applications. *Crystals* **2022**, *12*, 128. [CrossRef]
42. Kong, J.-Z.; Yin, L.; Xuan, Y.; Li, A.-D.; Wang, Q.-Z.; Zhou, F. Atomic layer-deposited Al_2O_3 interlayer for improved tribological and anti-corrosion properties of TiN hard coating on 316L stainless steel. *J. Mater. Eng. Perform.* **2019**, *28*, 7058–7067. [CrossRef]
43. Wang, P.C.; Cheng, T.C.; Lin, H.C.; Chen, M.J.; Lin, K.M.; Yeh, M.T. Effects of pre-sputtered Al interlayer on the atomic layer deposition of Al_2O_3 films on Mg–10Li–0.5Zn alloy. *Appl. Surf. Sci.* **2013**, *270*, 452–456. [CrossRef]
44. Wan, Z.; Zhang, T.F.; Ding, J.C.; Kim, C.-M.; Park, S.-W.; Yang, Y.; Kim, K.-H.; Kwon, S.-H. Enhanced corrosion resistance of PVD-CrN coatings by ALD sealing layers. *Nanoscale Res. Lett.* **2017**, *12*, 248. [CrossRef]
45. Härkönen, E.; Kolev, I.; Díaz, B.; Światowska, J.; Maurice, V.; Seyeux, A.; Marcus, P.; Fenker, M.; Toth, L.; Radnoczi, G.; et al. Sealing of hard CrN and DLC coatings with atomic layer deposition. *ACS Appl. Mater. Interfaces* **2014**, *6*, 1893–1901. [CrossRef]
46. Dai, W.; Wang, Q.; Kim, K.-H.; Kwon, S.-H. Al_2O_3/CrAlSiN multilayer coating deposited using hybrid magnetron sputtering and atomic layer deposition. *Ceram. Int.* **2019**, *45*, 11335–11341. [CrossRef]
47. Wan, Z.; Zhang, T.F.; Lee, H.-B.-R.; Yang, J.H.; Choi, W.C.; Han, B.; Kim, K.H.; Kwon, S.-H. Improved corrosion resistance and mechanical properties of CrN hard coatings with an atomic layer deposited Al_2O_3 interlayer. *ACS Appl. Mater. Interfaces* **2015**, *7*, 26716–26725. [CrossRef] [PubMed]
48. Kaady, E.; Alhussein, A.; Bechelany, M.; Habchi, R. Al_2O_3-ZnO atomic layer deposited nanolaminates for improving mechanical and corrosion properties of sputtered CrN coatings. *Thin Solid Films* **2022**, *759*, 139476. [CrossRef]
49. Hones, P. Structural and Electronic Properties of Transition Metal Nitride with Emphasis on Chromium Nitride Based Thin Films. Ph.D. Thesis, EPFL de Lausanne, Lausanne, Switzerland, 2000.

50. Kong, J.-Z.; Zhai, Q.-W.; Shen, J.-J.; Sun, X.-Y.; Cao, Y.-Q.; Xuan, Y.; Li, A.-D.; Wang, Q.-Z.; Zhou, F. Role of atomic layer deposited TiOxNy interlayer in tribological and corrosion properties of CrN coating. *Surf. Coat. Technol.* **2022**, *429*, 127981. [CrossRef]
51. Lasalmonie, A.; Strudel, J.L. Influence of grain size on the mechanical behaviour of some high strength materials. *J. Mater. Sci.* **1986**, *21*, 1837–1852. [CrossRef]
52. Kim, L.H.; Kim, K.; Park, S.; Jeong, Y.J.; Kim, H.; Chung, D.S.; Kim, S.H.; Park, C.E. Al_2O_3/TiO_2 nanolaminate thin film encapsulation for organic thin film transistors via plasma-enhanced atomic layer deposition. *ACS Appl. Mater. Interfaces* **2014**, *6*, 6731–6738. [CrossRef]
53. Mohamed, A.M.A.; Abdullah, A.M.; Younan, N.A. Corrosion behavior of superhydrophobic surfaces: A review. *Arab. J. Chem.* **2015**, *8*, 749–765. [CrossRef]

Disclaimer/Publisher's Note: The statements, opinions and data contained in all publications are solely those of the individual author(s) and contributor(s) and not of MDPI and/or the editor(s). MDPI and/or the editor(s) disclaim responsibility for any injury to people or property resulting from any ideas, methods, instructions or products referred to in the content.